 THIS PROJECT HAS RECEIVED FUNDING FROM THE FUEL CELLS AND HYDROGEN 2 JOINT UNDERTAKING (JU) UNDER GRANT AGREEMENT NO 101007170. THE JU RECEIVES SUPPORT FROM THE EUROPEAN UNION'S HORIZON 2020 RESEARCH AND INNOVATION PROGRAMME AND HYDROGEN EUROPE AND HYDROGEN EUROPE RESEARCH.

Material, Operating strategy and REliability optimisation for
LIFEtime improvements in heavy duty trucks

D3.1: Two primary catalyst concepts based on validated technology prepared

Public

DOCUMENT INFORMATION

Project	MORELife
Grant Agreement No.	N° 101007170
Deliverable No.	D3.1
Deliverable Title	Two primary catalyst concepts based on validated technology prepared
Dissemination Level	PU
Nature	R
Deliverable Version	V0.2
Deliverable Date	2021-10-28
Deliverable Responsible	Dr. Stanko Hočevar

AUTHORS/REVIEWERS TABLE

	Author(s) / Organization	**Date**
Written by	Dr. Stanko Hočevar/Mebius d.o.o.	2021-10-21
Reviewed by	Leonardo Astudillo, Franziska Hnyk – TUM	2021-10-27
Approved by	Coordinator / AVL	2021-10-28

CHANGE HISTORY

Version	**Who**	**Description**	**Date**
0.2	Hermine Pirker	Conversion of deliverable in new template – no content changes	2021-10-22
0.3	Leonardo Astudillo, Franziska Hnyk – TUM	Reviewed by	2021-10-27
0.4	Johannes Lackner AVL	Reviewed by	2021-10-28

Contents

Content of Figures

Content of Tables

1 Executive Summary

In this deliverable report we describe the two primary catalyst concepts based on validated technology prepared. State of the art achievements in projects similar to MORELife are presented and confronted with the present status of Mebius carbon supported Pt-skin over Cu3Pt intermetalic shell over CuxPt disordered alloy core catalyst. This catalyst will be used as a starting point in Phase 2 of the MORELife project and later, in Phase 3, developed further to obtain a breakthrough oxygen reduction reaction catalyst with BoL mass activity over 1.2 A/mgPt measured in single cell and high durability to achive the EoL mass activity higher than 80% of the BoL mass activity extrapolated over a period of 30.000 hours.

2 Deviations from original Description in the Grant Agreement Annex 1 Part A

2.1 Description of work related to deliverable in GA Annex 1 – Part A

However, with target PGM loadings commensurate with 0.3 g/kW at 1.2 W/cm2 (equating to 0.36 mg_{Pt}/cm^2 MEA), new materials need to be developed and implemented, as the end-of-life targets with performance losses of <10% can only be addressed through new and highly efficient catalysts. One of the approaches to maximise the platinum utilisation are core shell catalysts, in which the catalyst particle core is replaced by a cheaper material and only the shell consists of platinum. Thereby, the PGM loading is reduced without sacrificing performance. MEBs patented catalyst concept is promising and will be the starting point in the MORELife project.

MEB will use their proprietary catalyst with Pt-skin over PtCu3 Pm3m intermetallic shell over PtCux disordered alloy structured nanoparticles embedded in carbon support which contains only 25 at.% of PGM in the catalyst metal loading (11), and which exhibits a BoL mass activity (MA) of 1.15 A/mgPt (at 0.9 V and 100 kPa O_2) in single cell tests (12).

Task 3.1. Preparation of two primary catalyst concepts based on validated technology

Phase 2, lead: MEB, participants: TUM, UL, duration: M1-M18

Two catalysts synthesis Pt-Cu/Vulcan XC72 ex-situ chemically activated and Pt-Cu/KB EC300J ex-situ chemically activated in highly reproducible 2 g batches will be performed according to the synthesis procedure described in section 1.4. Complete characterisation of samples (HRTEM, STEM HAADF, XRD, ICP-MS, TF RDE, HUPD, CO striping) will follow.

2.2 Time deviations from original planning in GA Annex 1 – Part A

There are deviations with respect to timing of this deliverable.

The quantity of catalyst needed by TUM to be delivered by the end of M2 from the beginning of the project in the phase 2 of the project is 10 g of the Pt-Cu/Vulcan XC72 ex-situ chemically activated sample of the catalyst described in section 2.1.1. Due to the delay in delivery of the potassium tetrachloroplatinate salt from the U.K., purchased on October 6th, and delivered by FedEx, by 10 days, the synthesis of this sample will be delayed by 6 days but will not cause any further delay in the project.

2.3 Content deviations from original plan in GA Annex 1 – Part A

There are deviations from the Annex 1 – Part A with respect to the content.

Complete characterisation of samples (HRTEM, STEM HAADF, XRD, ICP-MS, TF RDE, HUPD, CO striping) will be delayed by 10 days. Instead of ICP-MS chemical analysis of the sample we shall use EDS analysis.

3 Introduction

Two main drivers for lowering the cost of the hydrogen-powered automotive proton exchange membrane fuel cell (PEMFC) system have been recognized: PEMFC stack platinum group metal (PGM) loading and its power density, both of which relate to oxygen reduction reaction (ORR) catalysis. Thus, the R&D is focused on synthesis and production of durable Pt-containing electrocatalysts for ORR with a mass activity higher than 1 A/mg_{Pt} measured in single cell tests, which would enable a PGM loading of 0.065 g_{PGM}/kW gross [James, D.B., 2017]. The most promising strategy towards enabling such high mass activities for ORR seems to be alloying of Pt-containing electrocatalysts with less expensive and less noble 3d transition metals (Cu, Co, and Ni, etc.) [Stonehart, P., 1990; He, Q., 2013; Stamenkovic, V.R., 2007; Toda, T., 1999; Katsounaros, I., 2014; Stephens, I.E.L, 2012; Mani, P., 2008]. When doing so, the mass activity for ORR is enhanced due to better utilization of Pt atoms [Stamenkovic, V.R., 2007; Huang, X., 2015; Chen, C., 2014; Choi, S., 2013] as well as due to higher intrinsic activity for ORR from a combination of the well-known ligand and strain effects [Stonehart, P., 1990; Toda, T., 1999; Stamenkovic, V., 2006; Strasser, P., 2010; Čolić, V., 2016]. On the other hand, the materials science community developing PEMFC electrocatalysts regularly faces serious issues when trying to transfer the high activities measured in ex situ tests, usually via the thin film rotating disc electrode (TF-RDE) method, to in situ membrane electrode assembly (MEA) PEMFC single cell tests [Stephens, I.E.L., 2016; Kongkanand, A., 2016; Mauger, S.A., 2018], in which high current densities at relatively low overpotentials are expected. The main issues related to this transfer are (i) the inability to scale-up the catalyst synthesis, (ii) the insufficient catalyst activation (leaching), (iii) the mass transport issues in the catalyst layer, (iv) the inability to prepare MEAs with optimized three-phase boundary, and (v) the presence of inhomogeneities in the catalyst layer [Stephens, I.E.L., 2016; Kongkanand, A., 2016]. Hence due to these reasons, promising MEA performances are momentarily scarce [Han, B., 2015; Garsany, Y., 2018]. Furthermore, it must be noted that for different electrocatalysts, the bottlenecks towards optimal MEA performance differ as well. For instance, non-noble electrocatalysts suffer from reactants mass transport issues as the catalyst layer is inevitably too thick due to the low active site density [Lee, K., 2014; Bezerra, C.W.B., 2008; Jaouen, F., 2018]. On the other hand, some catalysts with excellent RDE performance, for example, the 3M's nanostructured thin films (NSTF), suffer from flooding [Mauger, S.A., 2018], i.e., the inability to remove products (water) from the catalyst layer. Additionally, it was shown that some non-intrinsic parameters such as improved Nafion coverage and thinning of the membrane via a direct membrane deposition printing technique has an enormous effect on MEA performance at high current densities [Breitwieser, M., 2015; Klingele, M., 2015].

In this report, we present an evaluation of our proprietary $PtCu_3$ catalyst [Bele, M., 2014] characteristics obtained with TF-RDE and MEA tests. We show that the high ORR activity of the $PtCu_3$ electrocatalyst could potentially be transferred from an RDE to an MEA single cell test. The single cell measurements reveal one of the highest Pt-alloy electrocatalysts activities for ORR at 0.9 V. However, despite this excellent performance, it is demonstrated that at lower potentials, the electrochemical performance is still insufficient. Guidelines for improvement are given.

3.1 State of the art

Low temperature proton exchange fuel cell seem to be a promising alternative for replacing conventional energy infrastructure, especially for automobile applications. In general a fuel cell is an energy converter device, where fuel is directly converted to electricity. In theory this process is extremely efficient, in practice however, fuel cell efficiency is lowered due to several polarization losses among which a slow cathode reaction, namely oxygen reduction reaction is one of the major contriubutions of fuel cell efficieny limitations. A more active cathode catalyst is therefore inevitably needed to boost the kinetics of ORR.

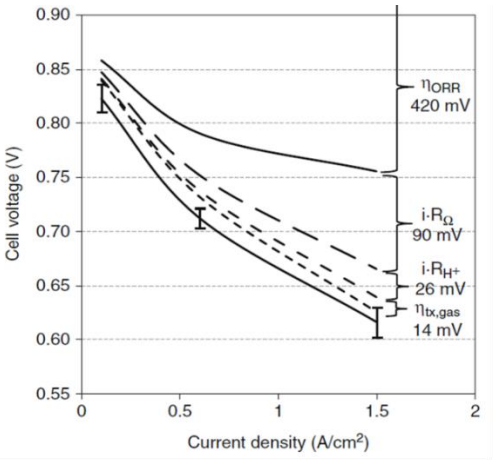

Figure 3-1 Typical voltage losses of LT PEMFC

Fig.3.1.1 presents the voltage loss terms in state-of-the-art H_2/air PEMFCs operated under representative automotive conditions [Gu W., 2009].

MEAs: 0.2/0.3 mg_{Pt}/cm^2 (anode/cathode) coated on an 18 µm thick composite membrane and sandwiched between 200 µm thick DMs (SGL 25BC). Operating conditions: H_2 and air stoichiometric flows of 2 and 1.8–5.5, respectively, stack pressure of 110–176 kPa_{abs}, gas inlet humidities of 30–60% RH, and stack temperature of 70–80°C.

The voltage loss caused by the slow ORR kinetics amounts to approximately 70% of the overall voltage loss.

In an automotive environment, catalyst must survive harsh transient (load cycling) operation of a vehicle. While Pt catalysts are very stable at the low electrode potentials occurring at the anode electrode (0 to 0.05), Pt dissolution poses significant concerns at the high electrode potentials occurring in the cathode electrode (≈0.7-0.95V vs. RHE). Several degradation phenomena are responsible for degradation of the catalyst layer such as: platinum dissolution and subsequent redeposition - Ostwald ripening, particle agglomeration via migration, carbon support corrosion leading to particle detachment and kolaps of the catalyst layer. Finally, platinum cations can diffuse into the membrane and precipitate in it. Figure 3.1.2 presents the catalyst degradation mechanisms and the cell voltage drop during start/stop cycling.

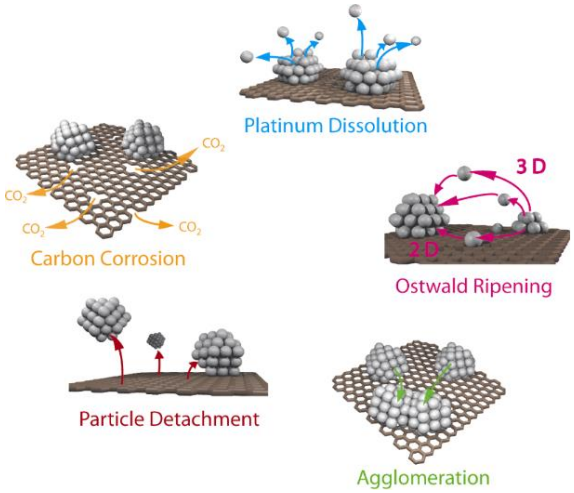

Figure 3-2 Mechanisms of catalyst degradation [Yu P., 2006]

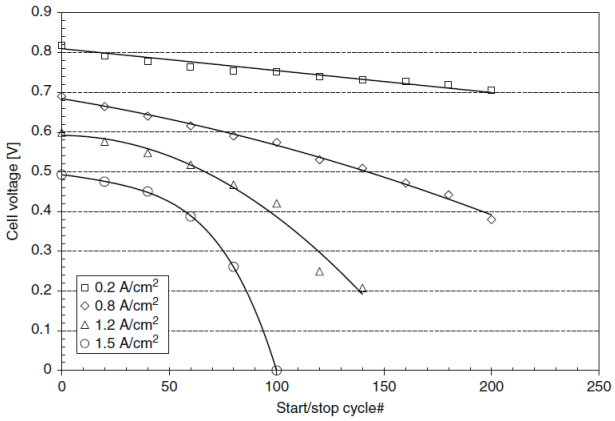

Figure 3-3 Cell voltage drop during start/stop cycling [Meier J.C., 2014]

Table 3-1 Single cell MEA characteristics at two operating conditions

Item	Units	2020 Target	2021 Status	
			94°C (250kPa)	80°C (150kPa)
Cost	$/kW$_{net}$	14	-	-
Q/ΔT	kW/°C	1.45	1.45	1.94
i at 0.8 V	A/cm²	0.3	0.44	0.30
PD at 670 mV	mW/cm²	1000	**1275**	**1000**
Durability	Hours @ < 10% V loss	5000	*5000-8000	2000-3600
Mass activity	A/mg$_{PGM}$	> 0.44	0.65	0.65
PGM Content	g/kW rated mg/cm²$_{MEA}$	0.125	0.10	0.125

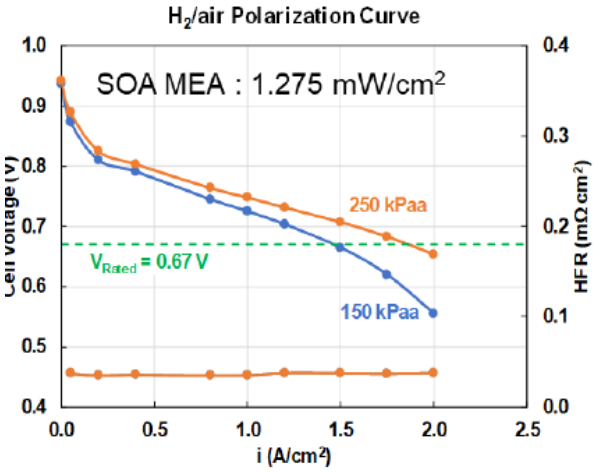

Figure 3-4 Polarization curves at two single cell operating conditions

ets

5000h – Approach to use benign operating conditions to prolong life successfully demonstrated using DOE drive cycle tests.

8000h - projected durability hours for UDDS/HWFET and DOE drive cycle using SOA MEA @ <0.125 mg_{Pt}/cm^2 (total).

Impact: Utilizing benign operating conditions is now considered to be an important tool to achieve even the much stringent heavy duty (HD) vehicle target requirements. [Kumaraguru S., 2021].

On the other hand, EERA has published the SoA (2020) and targeted (2030) parameters for fuel cell electrodes and catalysts (see Table 3-2).

Table 3-2 SoA and future targets for FC electrodes and catalysts [EERA, 2020]

No.	Parameter	Unit	Applicable conditions (e.g. *T*, *J*, #cycles, …)	SoA 2020	Target 2030
1	Area-Specific Resistance	Ωcm^2	At respective operation temperature	0.25	<0.1
2	Current density	A/cm^2	At respective operation temperature, 50 mV overpotential (FCanode) 100 mV (FC cathode)	0.3	0.8
3	Catalysts/electrode durability	hours	Under relevant operation conditions	5000-10000	>40000
4	Precious metal loading	mg/cm^2	Under relevant operation Conditions	0.25	<0.1

There are two FCH JU projects with the aim to develop advanced technology for fuel cell electric vehicles and to achieve high mass activity and durability of the fuel cell stacks: GAIA (2019) and INSPIRE (Start date 2016).

GAIA aims to developing a high performance automotive MEA that provides the materials and designs that satisfy the cost target by providing high power density at high current density, while also attaining the other essential objectives of durability, reliability and high operation temperature. Its intention is to:

- Realise the potential of these components in next generation MEAs showing a step-change in performance that will largely surpass the state of the art by delivering a beginning of life power density of 1.8 W/cm^2 at 0.6 V;
- Validate the MEA performance and durability in full size cell short stacks, with durability tests of 1,000 h with extrapolation to 6,000 h.
- Provide a cost assessment study that demonstrates that the MEAs can achieve the cost target of 6 €/kW for an annual production rate of 1 million square metres.

Pt and Pt alloy oxygen reduction reaction (ORR) electrocatalysts have been further advanced in the first 18 months of the GAIA project. The project targets for the ORR catalyst were to achieve a mass activity (MA) of at least 0.7 A/mg_{Pt} within an MEA and to maintain a surface area of at least 40 m^2/g_{Pt} after 30,000 cycles from 0.6 to 0.95 V.
At the start of the project, de-alloyed PtNi/C, octahedral PtNiIr/C and Pt-Rare Earth (RE) nanoparticle catalysts were identified as candidates to reach the project mass activity and surface area stability targets. TUB scaled up three octahedral PtNiIr/C catalyst variants from 20 mg to about 800 mg, at Pt loadings of 8% and 15% by weight on Vulcan XC72R carbon. The scaled octahedral PtNiIr/C alloys catalysts were evaluated in the rotating disk electrode (RDE) and demonstrated extremely high initial mass activities of up to 2.3 A/mg_{Pt} and electrochemical surface areas above 40 m^2/g_{Pt}. Three of these catalyst variants were sent to JMFC for testing in 50 cm^2 single cells but, unfortunately, in MEAs the MA was only about 0.30 A/mg_{Pt}.
Work at JMFC on carbon-supported de-alloyed 50% PtNi catalysts led to material with an average particle

size of 4.5 nm, as measured by transmission electron microscopy (TEM), and a surface area of about 65 m^2/g Pt. Performance testing in 50 cm^2 single cells gave a MA of 0.44 A/mg_{Pt} using a cathode loading of 0.20 mg Pt/cm^2, but a formulation tested at a reduced cathode loading of 0.10 mg Pt/cm^2 yielded an excellent MA of 0.89 A/mg_{Pt}. When this same catalyst was tested for durability in a 50 cm2 single cell using 30,000 cycles (0.6 – 0.925 V) at 80°C, the end of life surface area was 39 m^2/g_{Pt}, only marginally below the end of test target of 40 $m2/g_{Pt}$. This catalyst has therefore been considered to meet the targets set for this deliverable D4.3 (demonstration of a catalytic entity showing 0.7 A/mg_{Pt} in an MEA test and a surface area > 40 m^2/g_{Pt} after 30,000 cycles from 0.6 to 0.925 V) and will be progressed to WP5 for further evaluations. The Pt-RE catalysts being developed at CNRS, TUM and JMFC are also showing promise, with increased surface areas, but are at an earlier stage of development, and are therefore not included in this report [GAIA, 2020].

The objective of the INSPIRE project was to develop and integrate the most advanced critical PEMFC stack components, many from recent FCH JU programmes, into an automotive stack showing BOL performance of 1.5 W/cm2 at 0.6V, <10% power degradation after 6,000 hours, with a technical and economic assessment showing a cost of less than €50/kW at a 50,000 annual production scale.

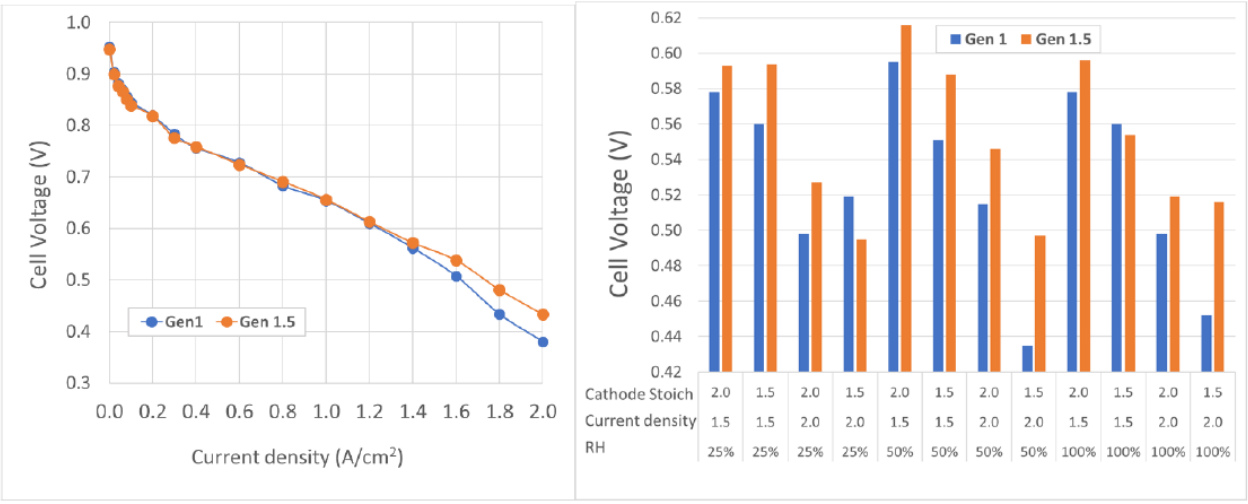

Figure 3-5 Comparison of single cell performances for two GDL types. Single cell tests (25 cm2) of GEN 1 and GEN 1.5/2/3. Left: Polarisation curve (JRC harmonised automotive conditions, MEA compression load 1 MPa, graphite serpentine plates). Right: Steady-state behaviour at different RH and cathode stoichiometry (H2/air 1.5 bar, 80°C, anode stoich = 1.5) [INSPIRE, 2019].

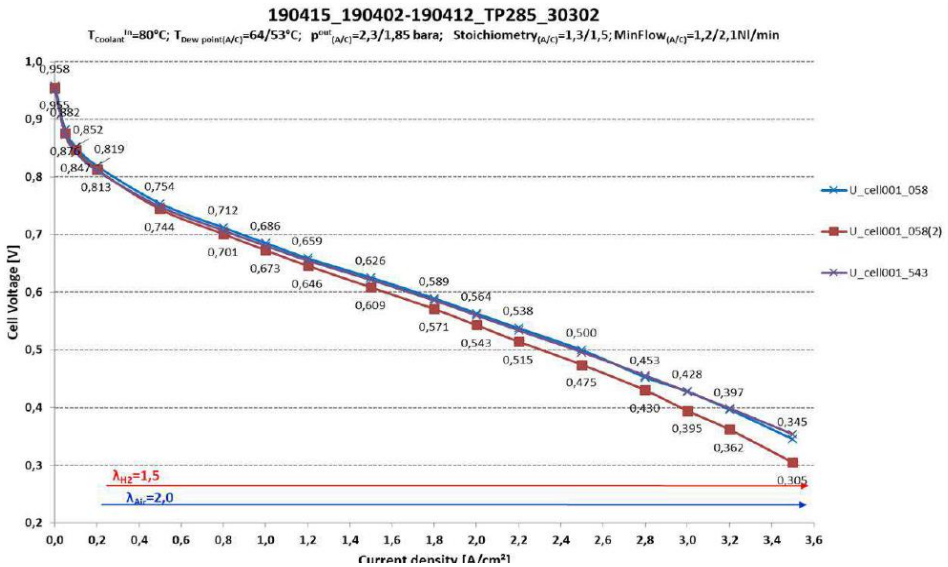

Figure 3-6 Polarization curve (H2/air) for TR0484 single cell measured in EU harmonised conditions

3.2 Concepts for the new catalyst development

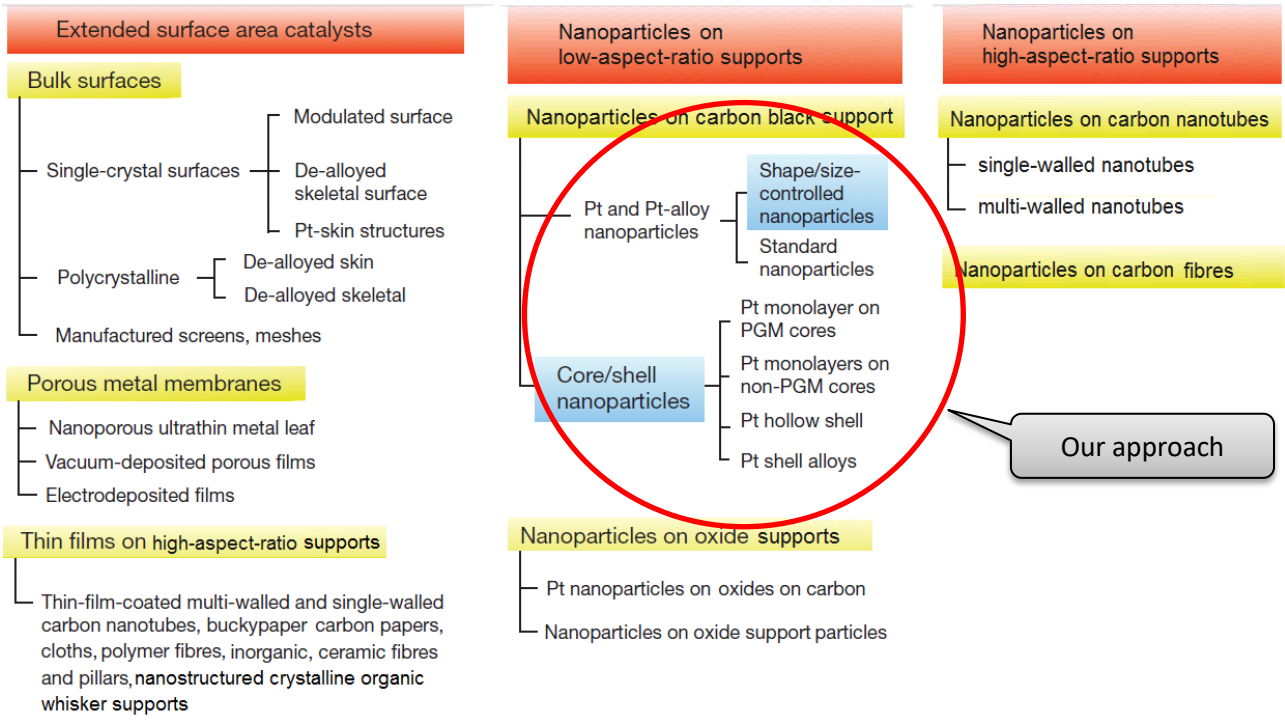

Figure 3-7 Mebius approach to the catalyst synthesis. Adapted from [Debe M., 2012].

Strategies for new catalysts synthesis

Increase PGM **specific area** by changing nanoparticles'

Increase PGM **utilization** by structuring the nanoparticles (core-shell, Pt-skin).

Decrease PGM **content** in the catalyst.

Less than **20 wt.%** Pt in the catalyst.

* PGM – platinum group

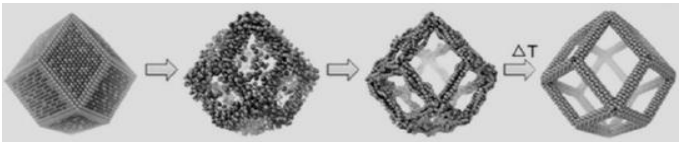

[Chen C., 2014]

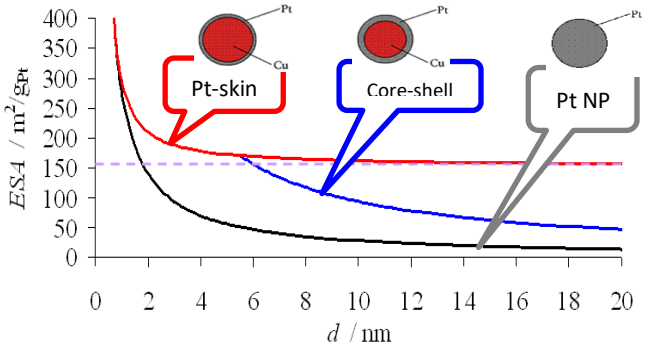

[Hodnik N., 2012]

Figure 3-8 Strategies for new catalysts synthesis

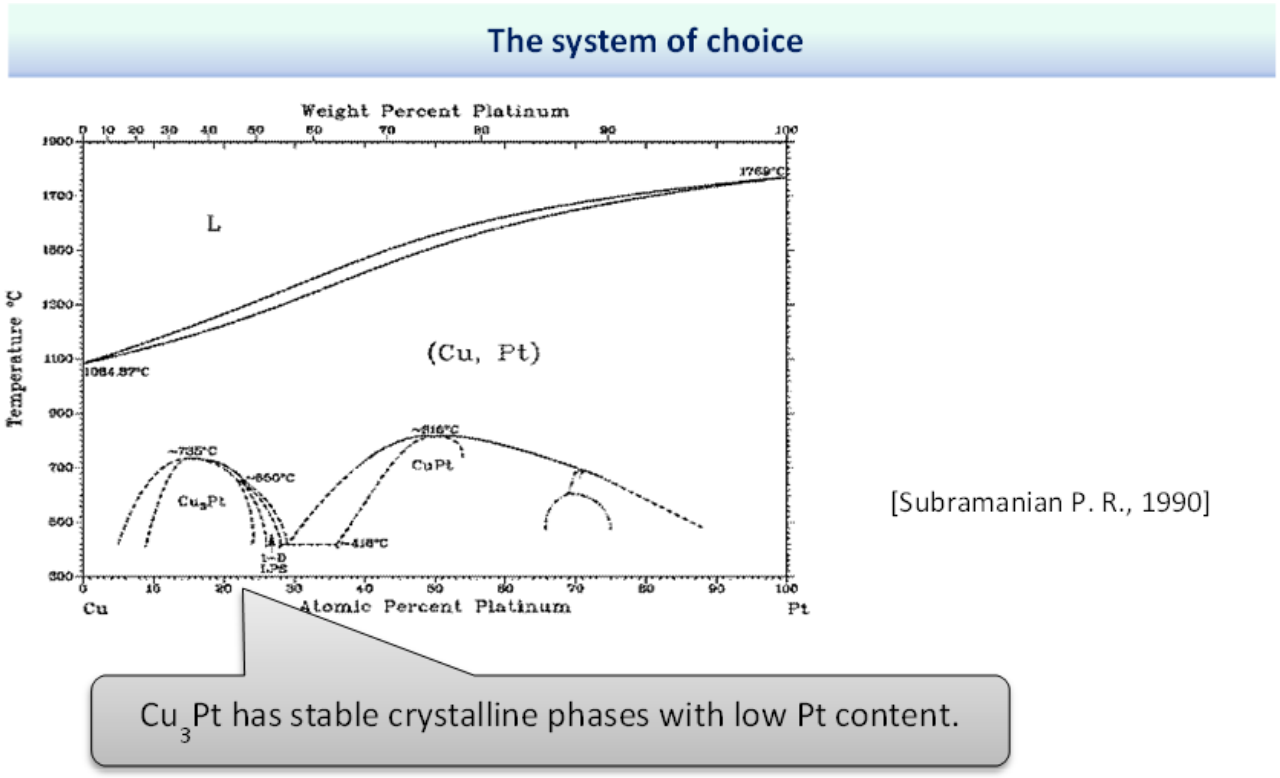

Figure 3-9 System of choice

3.3 Catalyst synthesis

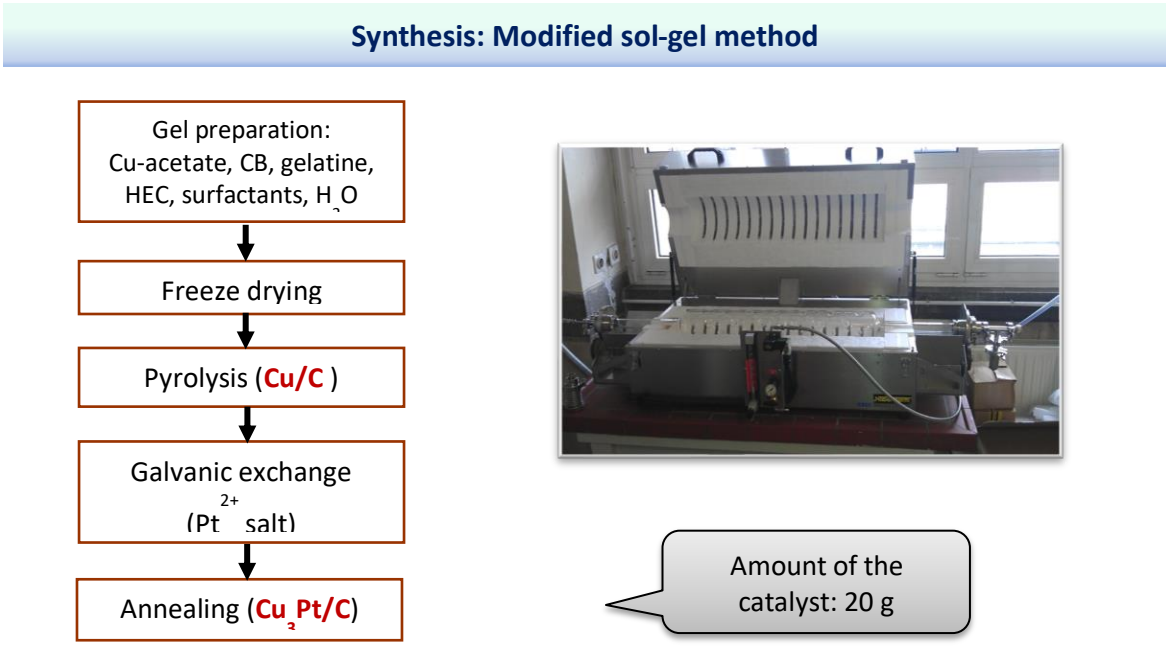

Figure 3-10 Description of catalyst synthesis process

[Bele M., 2015; Bele M., 2014; Hodnik N., 2012]

Characteristic XRD pattern of Cu-Pt alloys

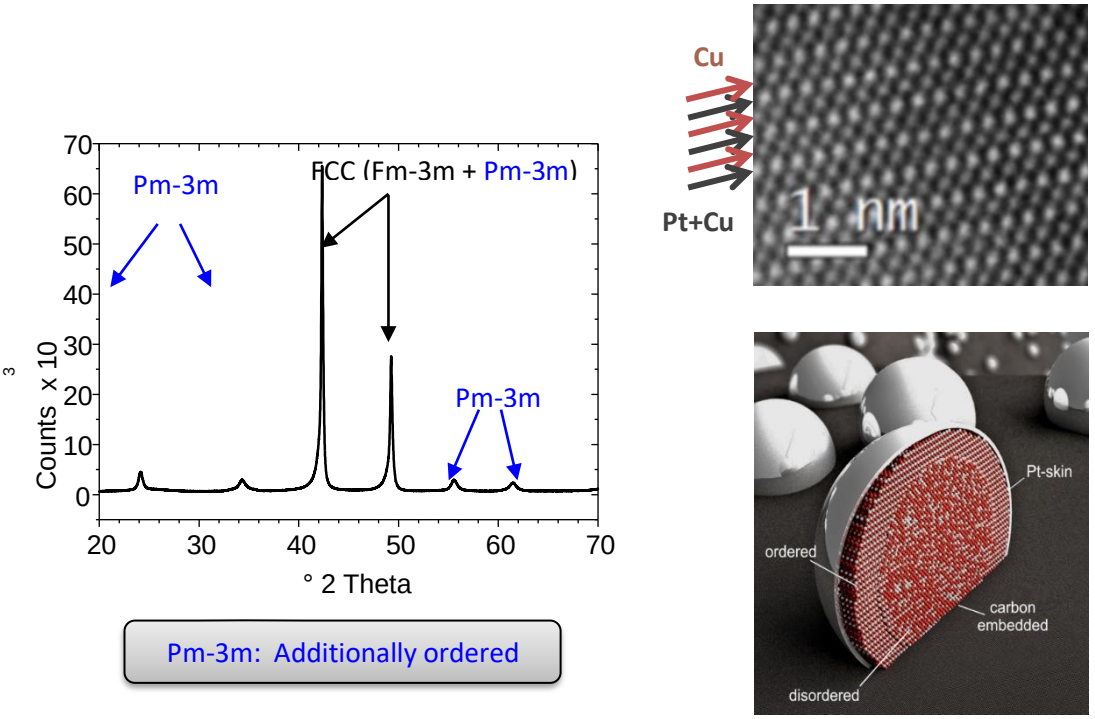

Figure 3-11 Description of catalyst structure

HR-STEM and EDX

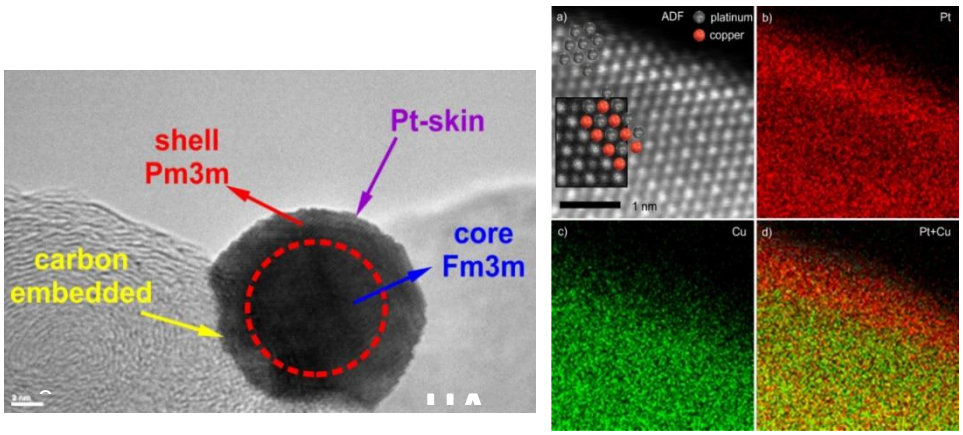

[Bele M., 2014]

The edge of nanoparticle shows Pt skin over Pm-3m shell.

Figure 3-12 Detailed structure of the catalyst nanoparticle

Effect of temperature on Cu-Pt ordering

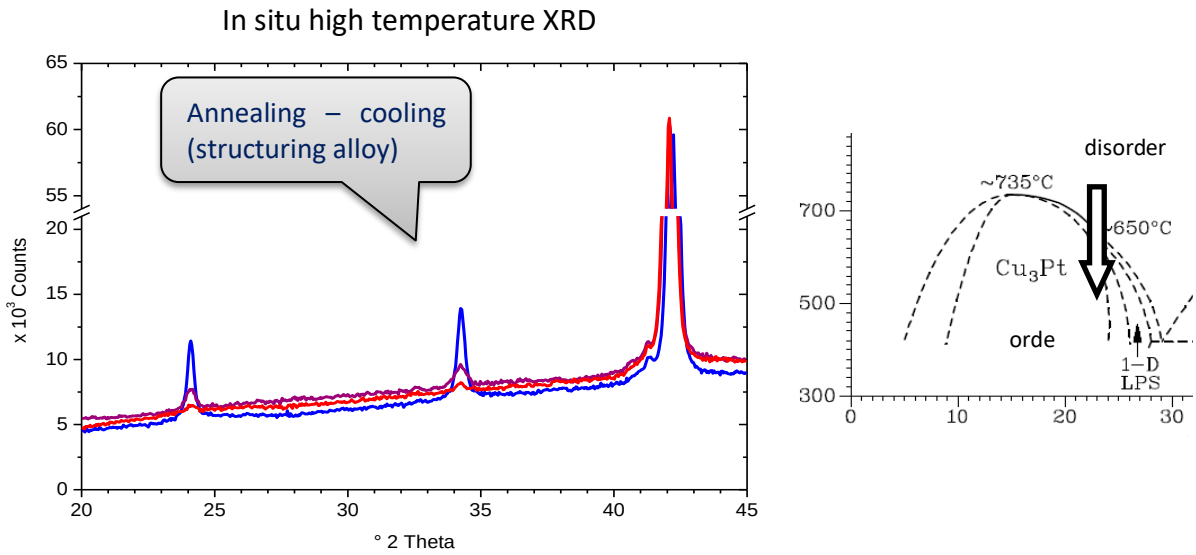

Figure 3-13 Description of cooling process during catalyst annealing to obtain ordered shell

3.4 Catalyst performance

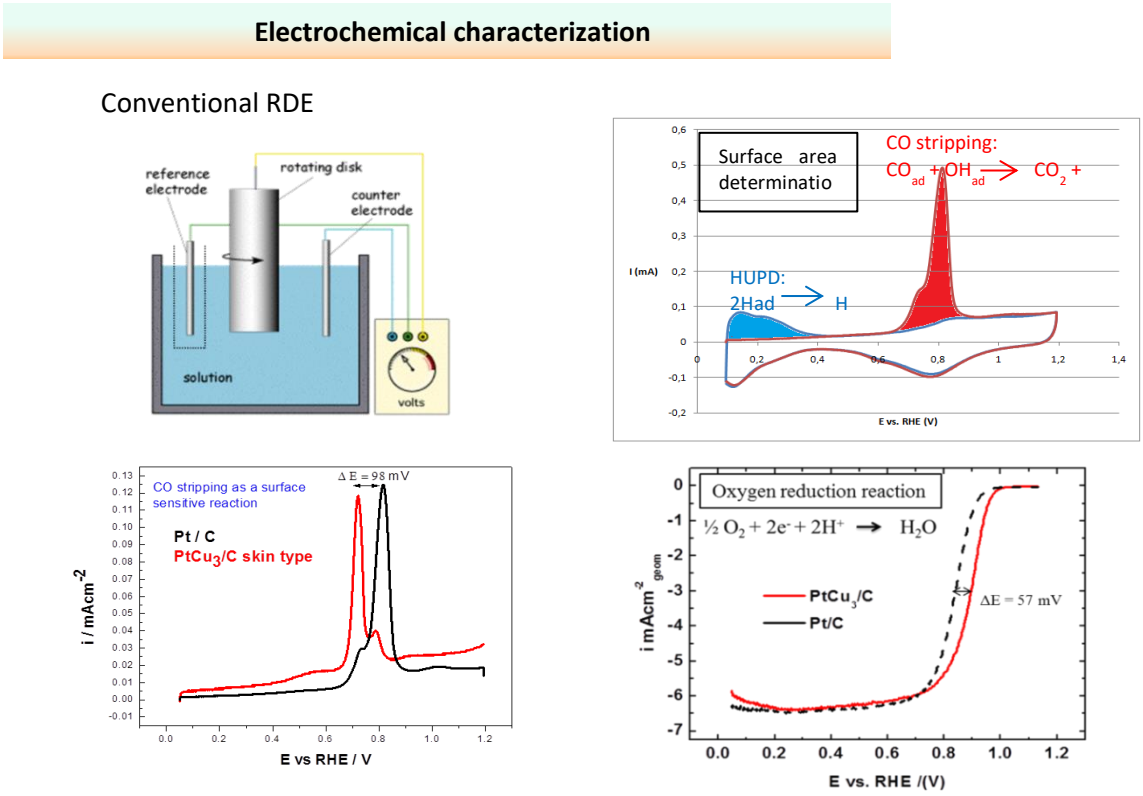

Figure 3-14 TF-RDE characteristics of the catalyst

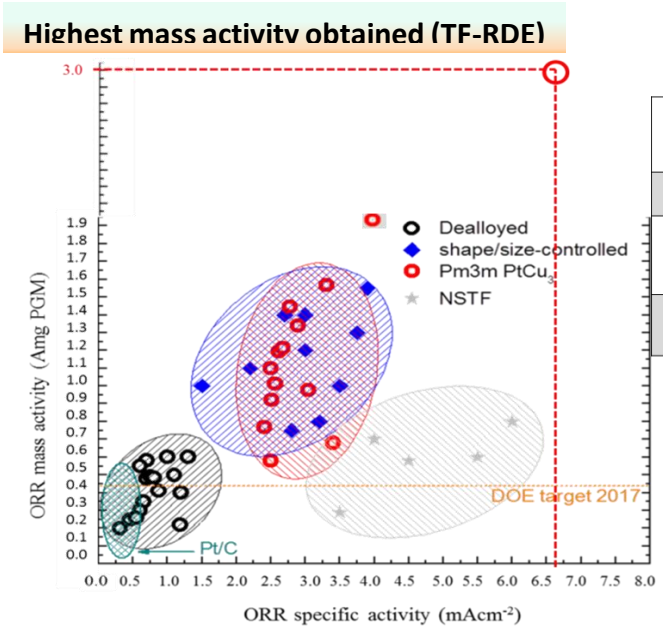

Sample	ECSA $m^2 g^{-1}$	Spec. Activity mA cm^{-2}	Mass activity A mg^{-1}
Cu_3Pt/C	47.4	4.11	1.95
Cu_3Pt/C milled	45.5	6.41	2.91
PtNi-nanoframe	NA	NA	5.7

* NA – not available

[Chen C., 2014]

Figure 3-15 RDE performance of synthesized catalyst. Adapted from: [Debe M., 2012]

Stability under cycling conditions (RDE)

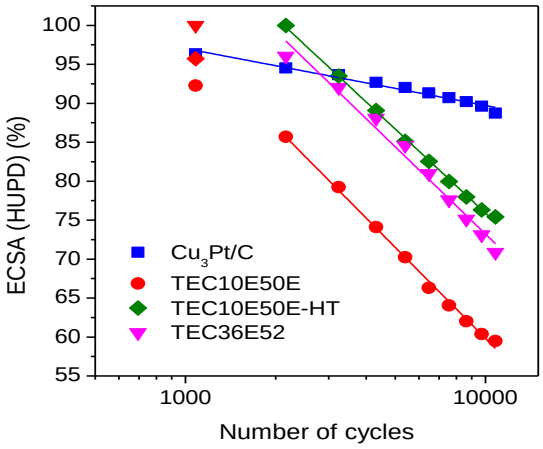

10800 cycles between 0.4 and 1.4 V_{RHE} with scan rate of 1V/s.
Every 1080 cycles 4 cycles of HUPD from 0.05 V to 1.2 V_{RHE} were measured consecutively with scan rate of 20 mV/s to determine ECSA.

The degradation slope of Cu_3Pt/C is 5-times smaller than the slopes for TKK catalysts!

Note: slopes for all TKK catalysts are equal.

Figure 3-16 Stability of Cu3Pt/C catalyst under cycling conditions in comparison with three TKK catalysts

Comparison of single cell measurements

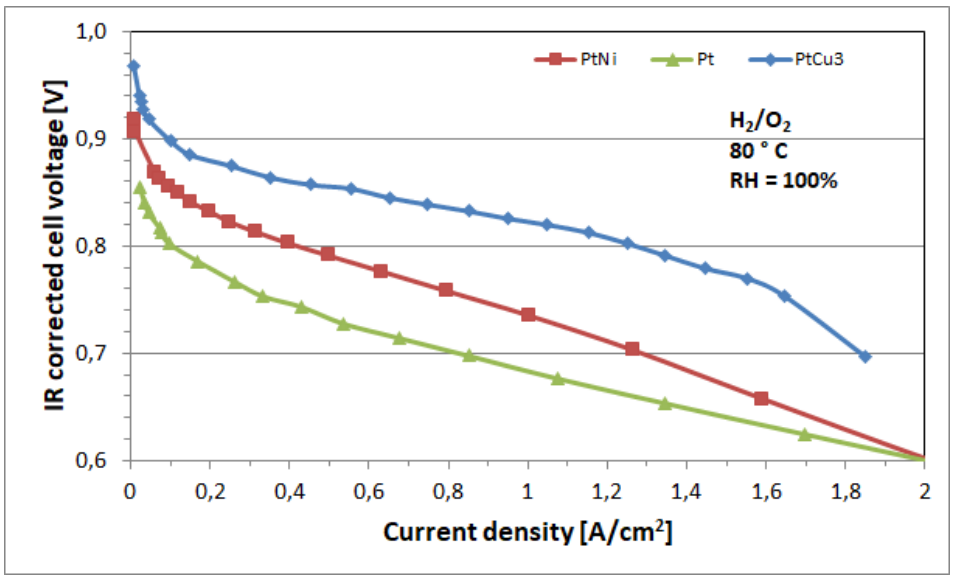

Figure 3-17 Comparison of IR corrected cell voltage for Pt/C, Pt-Ni nanoframes and Cu3Pt/C catalysts

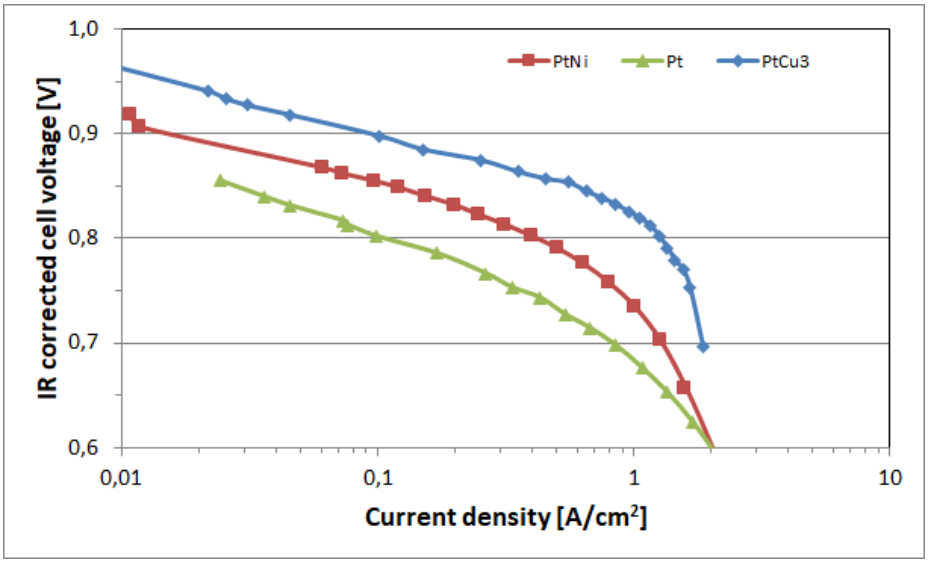

Figure 3-18 Comparison of Tafel plots for Pt/C, Pt-Ni nanoframes and Cu3Pt/C catalysts

Comparison of mass activities - single cell

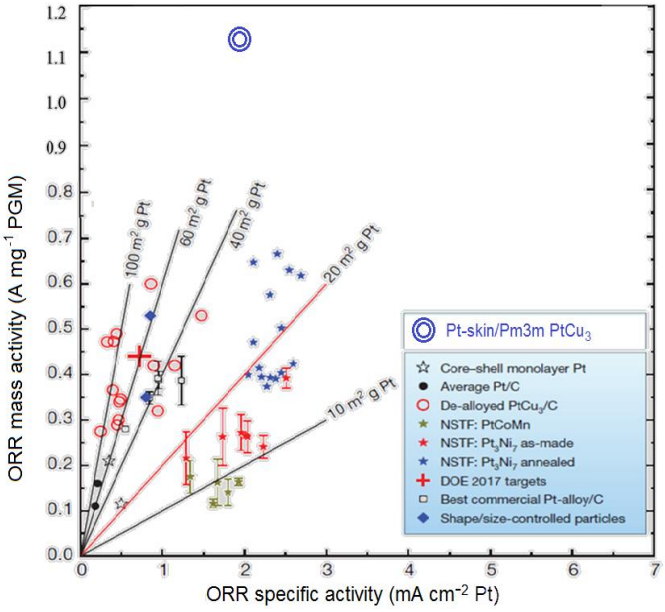

Adapted from: [Debe M., 2012]

Single cell tests: 25 cm^2

$L_{Pt,\ cath}$ = 0.09 mg_{Pt}/cm^2_{geom}

ECSA = 47 m^2/g_{Pt}

BoL SA (@ 0.9 $V_{iR\text{-}free}$) = 2.39 mA/cm^2_{Pt}

BoL MA (@ 0.9 $V_{iR\text{-}free}$) = 1.12 A/mg_{Pt}

Figure 3-19 Comparison of catalysts mass activities measured in single cell

4 Technical Section

4.1 Materials and Methods

4.1.1 Synthesis

4.1.1.1 $PtCu_3$/C Electrocatalyst Preparation

Intermetallic ordered $PtCu_3$ nanoparticles that are tightly embedded (anchored) into modified carbon support were prepared via the patented modified sol-gel synthesis using a gelatine precursor [Bele M., 2015; Bele M., 2014; Hodnik N., 2012; Hodnik N., 2014]. Briefly, the synthesis consists of two vital steps, the first being the annealing of a Cu salt precursor together with gelatine and carbon black to obtain Cu particles in a porous carbon matrix. In the second part, the Cu from the composite is partly galvanically displaced by a Pt precursor (K_2PtCl_4) and annealed for the second time. The "as-prepared" $PtCu_3$/C electrocatalyst was prepared according to a batch procedure that produced 20 g of catalyst.

4.1.1.2 Xero-Gel Preparation

To mix the reactant at the molecular level, first the 10 g of gelatine (GELATIN-B; Fluka, cat. No. 48722) and 0.9 g of cetyl-trimethyl-ammonium bromide (CTAB; Fluka, cat. No.52365) were dissolved in 250 mL of water at 60 °C while stirring, adding 12 g of copper acetate (Sigma-Aldrich, St. Louis, MI, USA; cat. No.25038) and 5 g of carbon black (VULCAN XC72R, CABOT, Italy,). A mixture was obtained, which was homogenized while stirring for 20 min, followed by an additional 10 min of stirring with a turbo-stirrer Ultra Turrax (15,000 rpm). Afterwards, the mixture was cooled to room temperature and left for 12 h. The obtained gel was freeze-dried with the use of liquid nitrogen and dried in vacuum to obtain a dried xerogel.

4.1.1.3 Pyrolysis

In the second step, dried xerogel was heated in a reduced atmosphere of H2 (5%)/Ar (gas flow rate 50 mL/min) at a rate 10 °C/min to 800 °C for 1 h and cooled to room temperature. After having been heat-treated, the composite of copper nanoparticles embedded in the porous matrix was ground.

4.1.1.4 Platination

Then followed platination of the composite using potassium tetrachloroplatinate (Sigma-Aldrich; St. Louis, MI, USA, cat. No. 323411), which had been dissolved in water solution while stirring. The addition of platinum precursor was performed in a two-step procedure. In the first step, 32% of the total amount was added dropwise to the composite of copper nanoparticles embedded in the carbon matrix. The obtained mixture was homogenized in an ultrasonic bath stirred for 15 min after which the rest of the platinum precursor was added. The mixture was stirred continuously for 12 h. Afterwards, the solid part of the mixture was separated from the liquid and washed three times with water and left to dry. The final composite material was obtained with annealing treatment.

4.1.1.5 Partial Oxidation

In the first heat treatment step, the partial oxidation of the platinized gel was adapted to control the amount of carbon on the catalyst nanoparticles. The composite material was first heat-treated in an air atmosphere at a heating rate of 5 °C/min to 310 °C and then left at this temperature for 1 h. With the partial oxidation process, nanoparticles buried within the support were uncovered, as well as the so-called carbon film on the nanoparticle surface was removed through controlled carbon oxidation. Subsequently, also removing the less stable carbon as sintering of very small particles was done to improve the corrosion resistance of the final $PtCu_3$/C catalyst due to very small particle sizes.

4.1.1.6 Annealing

After partial oxidation, the composite material was heated at a rate of 10 °C/min to 750 °C for 30 min for solid solution formation. The sample was then cooled to 500 °C at a rate of 3 °C/min, where it remained for the next 12 h. This step was necessary for the formation of the partially ordered crystal structure.

4.1.1.7 $PtCu_3$/C Electrocatalyst Acid Washing

As-prepared $PtCu_3$/C electrocatalyst (20 g) was subjected to a simple acid treatment in acetic acid (stirring in 1 M HAc for 6 h, followed by filtration). Filtered electrocatalyst was redispersed in Milli-Q water (Merck, Darmstadt, Germany, 18.2 MΩ cm) and stirred for 1 h before filtering. Washing in Milli-Q water was repeated four times to ensure the removal of any residual HAc and achieve a neutral pH. This catalyst was hereinafter denoted as $PtCu_3$/CA (A stands for Acid washed).

4.1.1.8 $PtCu_3$/CA Electrocatalyst Milling

$PtCu_3$/CA electrocatalyst (6 g) was subjected to a milling process. The milling was performed in a WAB Dyno®-mill Research Lab for 5 min at 3600 rpm in Ar purged hexane with 0.8 mm zirconium oxide balls. This catalyst was hereinafter denoted as $PtCu_3$/CAM (Acid washed + Milled).

4.1.2 X-ray Diffraction (XRD)

The powder X-ray diffraction (XRD) measurements of all samples were carried out on a Siemens D5000 diffractometer with Cu Kα1 radiation (λ = 1.5406 Å) in the 2ϑ range from 10° to 60° with the 0.04° step per 1 s. Samples were prepared on zero-background Si holder.

4.1.3 Transmission Electron Microscopy Analysis

A Cold-FEG JEOL-ARM microscope was used for the experiments. The microscope was operated at 200 kV with a camera length of 8 cm. The used probe current was approximately 14.5 pA. The electrocatalyst suspension (1 mg/ml) was ultrasonicated for 15 min and diluted 10 times (100 µL of the suspension, 900 µL of Milli-Q water). After an additional 5 min of ultrasonication (diluted suspension), 5 µL of the suspension was drop-casted on a finder gold grid. Once dried, the grid was inspected under a transmission electron microscope (TEM).

For Identical Location experiments, several spots were identified and imaged with scanning transmission electron microscopy (STEM) at different magnifications. Then the grid was removed from the microscope to perform the electrochemical experiments as follows: the grid was mounted on a glassy carbon disc, embedded in Teflon (Pine Instruments, Grove, PA, USA) with a geometric surface area of 0.196 cm^2. Prior to the electrochemical activation experiment, the electrode was polished to mirror the finish with Al_2O_3 paste (particle size 0.05 µm, Buehler) on a polishing cloth (Buehler, Lake Bluff, IL, USA). After polishing, the electrodes were rinsed and sonicated in Milli-Q water for 5 min. Electrochemical activation was conducted in a two-compartment electrochemical cell in a 0.1 M $HClO_4$ (Merck, Darmstadt, Germany, Suprapur, 70%, diluted by Milli-Q) electrolyte with a conventional three-electrode system controled by a potentiostat (Compact Stat, Ivium technologies, Houten, The Netherland). Ag|AgCl was used as a reference and a Pt wire as a counter electrode. The Ag|AgCl reference was separated from both the working and the counter electrode via a salt bridge in order to avoid Cl^- ion contamination. The electrode was mounted on the rotator (Pine Instruments). The electrode was placed in an Ar saturated electrolyte under potential control at 0.05 V (vs. RHE). The electrocatalyst on the Au-grid was potentio-dynamically treated for 200 cycles between 0.05–1.2 V_{RHE} with a scan rate of 300 mV s^{-1} and a 600 rpm rotation. All potentials were given against the reversible hydrogen electrode (RHE). After electrochemical treatment, the Au-grid was dipped into fresh Milli-Q water and left to dry at room temperature. Once dried, the grid was again inspected under TEM, tracking the areas previously identified by the letters and imaged for analysis. The images were taken under the same conditions as the previous ones.

4.1.4 Experimental ICP-MS Analysis

All reagents used were of analytical grade or better. For sample dilution and preparation of standards, ultrapure water (Milli-Q) and ultrapure acids (HNO_3 and HCl; Merck, Suprapur) were used. Standards were prepared in-house by the dilution of certified, traceable, inductively coupled plasma (ICP)-grade single-element standards (Merck CertiPUR). An Agilent Technologies 7900 ICP-mass spectrometry (MS) instrument, equipped with a MicroMist glass concentric nebulizer and Peltier-cooled, Scott type spray chamber was used. Prior to ICP-MS analysis, each sample was weighed (approximately 10 mg) and digested using a microwave-

assisted digestion system (CEM MDS-2000, Apeldoorn, The Netherland) in a solution of 6 mL HCl and 2 mL HNO_3. The digested samples were cooled to room temperature and then diluted with 2% v/v HNO_3 until their concentration was within the desired concentration range. After the digestion procedure, samples were centrifuged to yield clear solutions that were used in subsequent analyses.

4.1.5 Electrochemical Evaluation via Thin Film Rotating Disc Electrode (TF-RDE)

4.1.5.1 Preparation of Thin Films and the Setup

Electrochemical measurements were conducted in a two-compartment electrochemical cell in a 0.1 M $HClO_4$ (Merck, Suprapur, 70%, diluted by Milli-Q) electrolyte with a conventional three-electrode system controlled by a potentiostat (CompactStat, Iviumtechnologies). Ag|AgCl was used as a reference and a Pt wire as a counter electrode. The working electrode was a glassy carbon disc embedded in Teflon (Pine Instruments) with a geometric surface area of 0.196 cm^2. The Ag|AgCl reference was separated from both the working and the counter electrode via a salt bridge in order to avoid Cl^- ion contamination. Prior to each experiment, the two-compartment electrochemical cell was boiled in Milli-Q water for 1 h, and the electrode was polished to mirror finish with Al_2O_3 paste (particle size 0.05 µm, Buehler, Lake Blue, IL, USA) on a polishing cloth (Buehler). After polishing, the electrodes were rinsed and ultrasonicated (Ultrasound bath Iskra Sonis 4) in Milli-Q water for 5 min. 20 µL of 1 mg/mL water-based well-dispersed electrocatalyst ink was pipetted on the glassy carbon electrode completely covering it and dried under ambient conditions. After the drop had dried, 5 µL of Nafion solution (5% aqueous solution, Merck, Darmstadt, Germany) diluted in isopropanol (1:50) was added. Such preparation resulted in the electrocatalyst loading of 20 µg for all electrocatalysts and loading of approximately 22 $\mu g_{Pt}/cm^2_{geo}$. All potentials were given against the reversible hydrogen electrode (RHE), which was measured before the start of the experiment and at the end.

4.1.5.2 Electrochemical Evaluation in TF-RDE

After drying, the electrode was mounted on the rotator (Pine Instruments). The electrode was placed in an O_2 saturated electrolyte under open potential control (OCP) conditions. Ohmic resistance of the electrolyte was determined and compensated for as reported in reference [van der Vliet, D., 2010]. ORR polarization curves were measured with a rotation rate of 1600 rpm in the potential window 0.05–1.0 V_{RHE} with a scan rate of 20 mV s^{-1}. At the end of the ORR polarization curve measurement, the electrolyte was purged with CO under the potential of 0.05 V_{RHE} to ensure sufficient CO adsorption. Afterwards, the electrolyte was saturated with Ar. CO electrooxidation was performed using the same potential window and scan rate as in ORR, but without rotation and in an Ar-saturated electrolyte. The electrochemical surface area (ECSA) was determined by integrating the charge in CO electrooxidation experiments as described in reference [Mayrhofer, K.J.J., 2008]. After subtraction of background current due to capacitive currents, ORR kinetic parameters were calculated at 0.9 V_{RHE}. After this initial ORR characterization, electrocatalysts were subjected to an additional 200 cycles of electrochemical activation between 0.05 and 1.2 V_{RHE} with a scan rate of 300 mV s^{-1} under a rotation rate of 600 rpm. After this step, the electrolyte was exchanged for a fresh one. ORR polarization curves (including ohmic resistance and compensation) and CO electrooxidation measurements were performed again using the same process as in the initial ORR characterization.

4.1.6 Membrane Electrode Assembly (MEA) Preparation and Single Cell Studies

To evaluate the performance of the Pt-Cu cathode electro-catalysts in the single cell, at the anode side, a 40 wt% Pt/C (Hi-Spec 4000, Johnson Matthey, London, UK) catalyst was used in all experiments. The cathode catalytic ink was prepared by mixing, in an ultrasonic bath, the synthesized PtCu electrocatalyst with a 26 wt% of dry Aquivion® (Solvay, Brussels, Belgium, 20 wt% hydroalcoholic solution D79-20BS Solvay) as an ionomer. The catalytic ink was deposited onto a gas di*ff*usion layer SGL25BC by a spray coating. A Pt loading of 0.2 mg cm^2 was used for both anode and cathode. The MEAs were prepared

by hot pressing, assembling the electrodes with a 20 µm Short Side Chain (SSC) PFSA Aquivion membrane at 125 °C.

Electrochemical studies were performed in a 25 cm^2 single cell, at a temperature range between 80 °C and 95 °C, at 3 bar_{abs}, and 100% of relative humidity values (RH) as indicated. The cell was fed with H_2 as fuel and O_2 as an oxidant to evaluate simultaneously the single cell performance and the catalytic activity for the ORR. The flow rates were varied to have a constant stoichiometry of 2 or 4 and 1.5 or 3 for oxidant and fuel, respectively. The single cell performance was investigated by steady state galvanostatic measurements. The cell was connected to a fuel cell test station including an HP6051A electronic load. For the impedance analysis, the single cell was connected to a Potentiostat/Galvanostat PGSTAT30 AUTOLAB Metrohm (Utrecht, The Netherlands), equipped with a frequency response analyzer (FRA) module and a 20 A current booster. The impedance measurements were performed in the potentiostatic mode of fuel cell operation at 850 mV. The impedance spectra were obtained by varying the frequency of the voltage perturbation signal from 0.1 Hz to 100 kHz, by using an amplitude 10 mV for the perturbing signal.

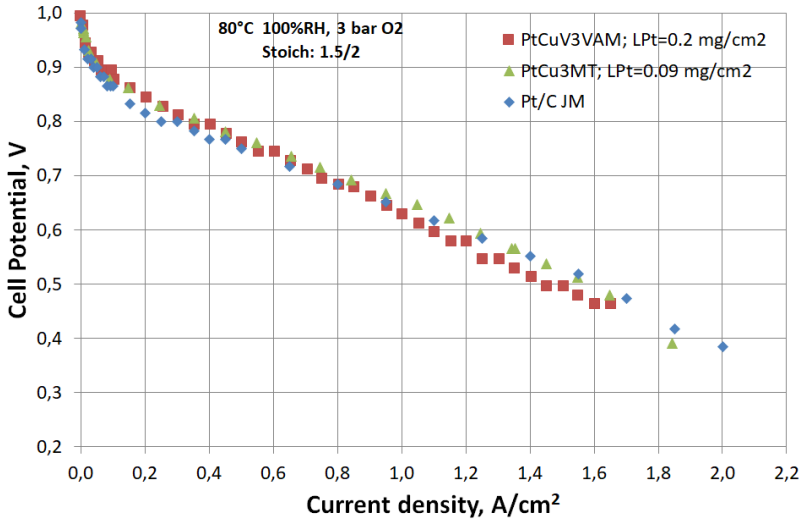

Figure 4-1. Single cell H_2/O_2 polarization curves for two PtCu/C cathode catalyst samples with different Pt loadings and for the reference catalyst Hi-Spec 4000 (JM, UK)

The BoL mass activity of the PtCuV3VAM catalyst sample obtained was 0.533 A/mg_{Pt}, and the mass activity of the PtCu3MT catalyst sample obtained was 1.12 $A/mg_{Pt.}$ This type of catalyst will be used as a starting point for further catalyst improvement in the MORELife project.

5 Summary and Conclusion

Analysis of proprietary $PtCu_3$ ORR catalyst was performed by using structural and electrochemical methods. Single-cell measurements at an operating temperature of 95 °C [Bele M., 2019], which is the targeted temperature for automotive applications, reveal that the beginning-of-life (BoL) catalyst performances show a promising step towards the US DOE performance targets for 2020 at low current density, and enable the preparation of low Pt loading cathodes. This represents a great foundation for the potential application of the Pt-Cu system in the MEA arrangement. The challenge of achieving high current densities, however, remains to be solved. It is very likely that in the present catalyst the main obstacle is the oxygen mass transport in the microporous carbon support, as indirectly confirmed by the analysis of polarization curves with the Kulikovsky model. As a consequence, the cell voltage at the rated power is about 130 mV lower than the targeted performance. Further optimization of the catalyst synthesis parameters, pre-treatment, and MEA production is underway.

6 Terms, Abbreviations and Definitions

MORELife	Material, Operating strategy and REliability optimisation for LIFEtime improvements in heavy duty trucks
CO	Confidential, restricted under conditions set out in Model Grant Agreement - only for members of the consortium (including the JU).
DEC	Websites, patents filing, press & media actions, videos, etc.
DEM	Demonstrator, pilot, prototype, plan designs
HW	Hardware
R	Report
OTHER	Other
PU	Public, fully open, e.g. web
WP	Work Package
PEMFC	Proton Exchange Membrane Fuel Cell
MEA	Membrane-Electrode Assembly
ICP-MS	Inductively Coupled Plasma Mass Spectrometry
RDE	Rotating Disc Electrode
TF-RDE	Thin Film Rotating Disc Electrode
XRD	X-Ray Diffraction
HRTEM	High-Resolution Transmission Electron Microscopy
STEM	Scanning/Transmission Electron Microscopy
HAADF	High Angle Annular Dark Field
HUPD	Hydrogen Underpotential Deposition
SA	Specific Activity
MA	Mass Activity
ECSA	Electrochemical Surface Area
EDS	Energy Dispersive Spectroscopy
GDL	Gas Diffusion Layer
MPL	Microporous Layer
PEM	Proton Exchange Membrane
IJP	Inkjet Printing
LDV	Light Duty Vehicle
HDV	Heavy Duty Vehicle
BoL	Beginning of Life

Table 6-1: Terms, Abbreviations and Definitions

7 References

James, D.B., 2017	James, D.B.; Huya-Kouadio, M.J.; Houchins, C.; DeSantis, A.D. Mass Production Cost Estimation of Direct H2 PEM Fuel Cell Systems for Transportation Applications: 2017 Update; Technical Report; Strategic Analysis Inc.: Arlington, VA, USA, 2017.
Stonehart, P., 1990	Stonehart, P. Development of Advanced Noble Metal-Alloy Electrocatalysts for Phosphoric Acid Fuel Cells (PAFC). Berichte der Bunsengesellschaft für Phys. Chemie 1990, 22, 913–921.
He, Q., 2013	He, Q.; Shyam, B.; Nishijima, M.; Yang, X.; Koel, B.; Ernst, F.; Ramaker, D.; Mukerjee, S. Highly Stable Pt–Au@Ru/C Catalyst Nanoparticles for Methanol Electro-oxidation. J. Phys. Chem. C 2013, 117, 1457–1467
Stamenkovic, V.R., 2007	Stamenkovic, V.R.; Fowler, B.; Mun, B.S.; Wang, G.; Ross, P.N.; Lucas, C.A.; Marković, N.M.; Markovic, N.M. Improved oxygen reduction activity on Pt3Ni(111) via increased surface site availability. *Science* 2007, *315*, 493–497.
Toda, T., 1999	Toda, T.; Igarashi, H.; Uchida, H.;Watanabe, M. Enhancement of the Electroreduction of Oxygen on Pt Alloys with Fe, Ni, and Co. J. Electrochem. Soc. 1999, 146, 3750–3756.
Katsounaros, I., 2014	Katsounaros, I.; Cherevko, S.; Zeradjanin, A.R.; Mayrhofer, K.J.J.; Karl, J.J. Oxygen electrochemistry as a cornerstone for sustainable energy conversion. *Angew. Chem. Int. Ed. Engl.* 2014, *53*, 102–121.
Stephens, I.E.L, 2012	Stephens, I.E.L.; Bondarenko, A.S.; Grønbjerg, U.; Rossmeisl, J.; Chorkendorff, I. Understanding the electrocatalysis of oxygen reduction on platinum and its alloys. *Energy Environ. Sci.* 2012, *5*, 6744–6762.
Mani, P., 2008	Mani, P.; Srivastava, R.; Strasser, P. Dealloyed Pt–Cu Core–Shell Nanoparticle Electrocatalysts for Use in PEM Fuel Cell Cathodes. *J. Phys. Chem. C* 2008, *112*, 2770–2778.
Huang, X., 2015	Huang, X.; Zhao, Z.; Cao, L.; Chen, Y.; Zhu, E.; Lin, Z.; Li, M.; Yan, A.; Zettl, A.; Wang, Y.M.; et al. High-performance transition metal-doped Pt3Ni octahedra for oxygen reduction reaction. *Science* 2015, *348*, 1230–1234.
Chen, C., 2014	Chen, C.; Kang, Y.; Huo, Z.; Zhu, Z.; Huang, W.; Xin, H.L.; Snyder, J.D.; Li, D.; Herron, J.A.; Mavrikakis, M.; et al. Highly crystalline multimetallic nanoframes with three-dimensional electrocatalytic surfaces. *Science* 2014, *343*, 1339–1343.
Choi, S., 2013	Choi, S.; Xie, S.; Shao, M.; Odell, J.H.; Lu, N.; Peng, H.-C.; Protsailo, L.; Guerrero, S.; Park, J.; Xia, X.; et al. Synthesis and Characterization of 9 nm Pt–Ni Octahedra with a Record High Activity of 3.3 A/mg. *Nano Lett.* 2013, *13*, 3420–3425.
Stamenkovic, V., 2006	Stamenkovic, V.; Mun, B.S.; Mayrhofer, K.J.J.J.; Ross, P.N.; Markovic, N.M.; Rossmeisl, J.; Greeley, J.; Nørskov, J.K. Changing the activity of electrocatalysts for oxygen reduction by tuning the surface electronic structure. *Angew. Chemie (International ed.)* 2006, *45*, 2897–2901.
Strasser, P., 2010	Strasser, P.; Koh, S.; Anniyev, T.; Greeley, J.; More, K.; Yu, C.; Liu, Z.; Kaya, S.; Nordlund, D.; Ogasawara, H.; et al. Lattice-strain control of the activity in dealloyed core-shell fuel cell catalysts. Nat. Chem. 2010, 2, 454–460
Čolić, V., 2016	Čolić, V.; Bandarenka, A.S. Pt Alloy Electrocatalysts for the Oxygen Reduction Reaction: From Model Surfaces to Nanostructured Systems. *ACS Catal.* 2016, *6*, 5378–5385.
Stephens, I.E.L., 2016	Stephens, I.E.L.; Rossmeisl, J.; Chorkendorff, I. Toward sustainable fuel cells. *Science* 2016, *354*, 1378–1379.
Kongkanand, A., 2016	Kongkanand, A.; Mathias, M.F. The Priority and Challenge of High-Power Performance of Low-Platinum Proton-Exchange Membrane Fuel Cells. *J. Phys. Chem. Lett.* 2016, *7*, 1127–1137.
Mauger, S.A., 2018	Mauger, S.A.; Neyerlin, K.C.; Alia, S.M.; Ngo, C.; Babu, S.K.; Hurst, K.E.; Pylypenko, S.; Litster, S.; Pivovar, B.S. Fuel Cell Performance Implications of Membrane Electrode Assembly Fabrication with Platinum-Nickel Nanowire Catalysts. *J. Electrochem. Soc.* 2018, *165*, 238–245.
Han, B., 2015	Han, B.; Carlton, C.E.; Kongkanand, A.; Kukreja, R.S.; Theobald, B.R.; Gan, L.; O'Malley, R.; Strasser, P.; Wagner, F.T.; Shao-Horn, Y. Record activity and stability of dealloyed bimetallic catalysts for proton exchange membrane fuel cells. *Energy Environ. Sci.* 2015, *8*, 258–266.
Garsany, Y., 2018	Garsany, Y.; Atkinson, R.W.; Gould, B.D.; Swider-Lyons, K.E. High power, Low-Pt membrane electrode assemblies for proton exchange membrane fuel cells. *J. Power Sources* 2018, *408*, 38–45.
Lee, K., 2014	Lee, K.; Alonso-Vante, N.; Zhang, J. Transition Metal Chalcogenides for Oxygen Reduction Electrocatalysts in PEM Fuel Cells. In *Non-Noble Metal Fuel Cell Catalysts*; Wiley-VCH Verlag

	GmbH & Co. KGaA: Weinheim, Germany, 2014; Volume 9783527333, pp. 157–182. ISBN 9783527664900.
Bezerra, C.W.B., 2008	Bezerra, C.W.B.; Zhang, L.; Lee, K.; Liu, H.; Marques, A.L.B.; Marques, E.P.; Wang, H.; Zhang, J. A review of Fe-N/C and Co-N/C catalysts for the oxygen reduction reaction. *Electrochim. Acta* 2008, *53*, 4937–4951.
Jaouen, F., 2018	Jaouen, F.; Jones, D.; Coutard, N.; Artero, V.; Strasser, P.; Kucernak, A. Toward Platinum Group Metal-Free Catalysts for Hydrogen/Air Proton-Exchange Membrane Fuel Cells. *Johnson Matthey Technol. Rev.* 2018, *62*, 231–255.
Breitwieser, M., 2015	Breitwieser, M.; Klingele, M.; Britton, B.; Holdcroft, S.; Zengerle, R.; Thiele, S. Improved Pt-utilization efficiency of low Pt-loading PEM fuel cell electrodes using direct membrane deposition. *Electrochem. Commun.* 2015, *60*, 168–171.
Klingele, M., 2015	Klingele, M.; Breitwieser, M.; Zengerle, R.; Thiele, S. Direct deposition of proton exchange membranes enabling high performance hydrogen fuel cells. *J. Mater. Chem. A* 2015, *3*, 11239–11245.
Bele, M., 2014	Bele, M.; Gaberšček, M.; Kapun, G.; Hodnik, N.; Hočevar, S. Electrocatalytic composite(s), associated composition(s) and associated process(es). European Patent Application EP2735044, 25 March 2014.
Gu W., 2009	Gu W, Baker DR, Liu Y, Gasteiger HA (2009) Proton exchange membrane fuel cell (PEMFC) down-the-channel performance model. In: Vielstich W, Gasteiger HA, Yokokawa H (eds) Handbook of fuel cells – advances in electrocatalysis, materials, diagnostics, and durability, vol 5. Wiley, Chichester,pp 631–657
Yu P., 2006	P, Yu et al. *ECS Trans*, 2006, *3*, 797–809.
Meier, J.C., 2014	Meier, J.C. et al. *Beilstein J. Nanotechnol*. 2014, *5*, 44–67)
Kumaraguru S., 2021	Kumaraguru S. (PI), General Motors Company, Global Fuel Cell Business, Durable High-Power Membrane Electrode Assembly with Low Pt Loading, Presentation at DOE Hydrogen Program 2021 Annual Merit Review and Peer Evaluation Meeting
EERA, 2020	Key performance indicators (KPIs) for FCH research and innovation, 2020 – 2030, Version: 5.0, Last update 06/08/2020, EERA, JP FCH, HER, FCH JU
GAIA, 2020	FCH JU Project GAIA, D4.3: DEMONSTRATION OF A CATALYTIC ENTITY SHOWING 0.7 A/mgPt, IN AN MEA TEST AND A SURFACE AREA > 40 m2 /gPt AFTER 30,000 CYCLES FROM 0.6 TO 0.925 V, Deliverable Report, 30th October 2020; https://www.gaia-fuelcell.eu/index.php/activities/deliverables
INSPIRE, 2019	FCH JU Project INSPIRE, D4.4 – FINAL MEA DESIGN ACHIEVING TARGET PERFORMANCE (1.5 WCM-2) AND DURABILITY Deliverable Report Version 1.0 – 07/11/2019
Chen C., 2014	C. Chen, P. Yang and V. Stamenkovic, Science, 2014, 343, 1339
Hodnik N., 2012	Hodnik N. Et al., Energy Procedia 29 (2012) 208 – 215
Debe M., 2012	Debe M., Nature 486 (2012) 43-51
Subramanian P. R., 1990	Subramanian P. R. & Laughlin, D. E. In: Binary Alloy Phase Diagrams 2nd edn, Vol. 2 (ed.: Massalski, T. B.), ASM International 1990, 1460–1462, ISBN: 978-0-87170-403-0
Bele M., 2015	M. Bele, M. Gaberšček, G. Kapun, N. Hodnik, S, Hočevar *US Patent No:* 9147885 B2 (2015)
Bele M., 2014	Bele, M.; Jovanovič, P.; Pavlišič, A.; Jozinović, B.; Zorko, M.; Rečnik, A.; Chernyshova, E.; Hočevar, S.; Hodnik, N.; Gaberšček, M. A highly active PtCu3 intermetallic core-shell, multilayered Pt-skin, carbon embedded electrocatalyst produced by a scale-up sol-gel synthesis. *Chem. Commun. (Camb.)* 2014, *50*, 13124–13126.
Hodnik N., 2012	Hodnik, N.; Bele, M.; Hočevar, S. New Pt-skin electrocatalysts for oxygen reduction and methanol oxidation reactions. *Electrochem. Commun.* **2012**, *23*, 125–128.
Hodnik N., 2014	Hodnik, N.; Jeyabharathi, C.; Meier, J.C.; Kostka, A.; Phani, K.L.; Rečnik, A.; Bele, M.; Hočevar, S.; Gaberšček, M.; Mayrhofer, K.J.J. Effect of ordering of PtCu3 nanoparticle structure on the activity and stability for the oxygen reduction reaction. *Phys. Chem. Chem. Phys.* 2014, *16*, 13610–13615.

van der Vliet, D., 2010	van der Vliet, D.; Strmcnik, D.S.; Wang, C.; Stamenkovic, V.R.; Markovic, N.M.; Koper, M.T.M.M. On the importance of correcting for the uncompensated Ohmic resistance in model experiments of the Oxygen Reduction Reaction. J. Electroanal. Chem. 2010, 647, 29–34.
Mayrhofer, K.J.J., 2008	Mayrhofer, K.J.J.; Strmcnik, D.; Blizanac, B.B.; Stamenkovic, V.; Arenz, M.; Markovic, N.M. Measurement of oxygen reduction activities via the rotating disc electrode method: From Pt model surfaces to carbon-supported high surface area catalysts. Electrochim. Acta 2008, 53, 3181–3188.
Bele M., 2019	Bele M., Gatalo M., Jovanovič P., Ruiz-Zepeda F., Šala M., Šest E., Hodnik N., Hocˇevar S., Gatto I., Saccà A., Aricò A.S. and Gaberščˇek M., Insight on Single Cell Proton Exchange Membrane Fuel Cell Performance of Pt-Cu/C Cathode, *Catalysts* 2019, *9*, 544.